Medical Image Fusion and Denoising with Alternating Sequential Filter and Adaptive Fractional Order Total Variation

Wenda Zhao and Huchuan Lu, *Senior Member, IEEE*

***Abstract*— Medical image fusion aims at integrating information from multimodality medical images to obtain a more complete and accurate description of the same object, which provides an easy access for image-guided medical diagnostic and treatment. Unfortunately, medical images are often corrupted by noise in acquisition or transmission, and the noise signal is easily mistaken for a useful characterization of the image, making the fusion effect drop significantly. Thus, the existence of noise presents a great challenge for most of traditional image fusion methods. To address this problem, an effective variation model for multimodality medical image fusion and denoising is proposed. First, a multiscale alternating sequential filter is exploited to extract the useful characterizations (e.g., details and edges) from noisy input medical images. Then, a recursive filtering-based weight map is constructed to guide the fusion of main features of input images. Additionally, total variation (TV) constraint is developed by constructing an adaptive fractional order p based on the local contrast of fused image, further effectively suppressing noise while avoiding the staircase effect of the TV. The experimental results indicate that the proposed method performs well with both noisy and normal medical images, outperforming conventional methods in terms of fusion quality and noise reduction.**

***Index Terms*— Adaptive fractional order total variation (AFOTV), medical image fusion and denoising, multiscale alternating sequential filter, variation model.**

I. Introduction

MEDICAL image fusion attracts much attention in the recent years due to being a vital component of machine vision. It is a significant technology for diagnostics and treatments in the field of medical instrumentation and measurement [1]. It is based on the fact that each imaging modality reports on a restricted domain and provides information in limited domains that some are common and some are unique [2]. For instance, computed tomography (CT) image provides the best information on dense structures with less distortion like bones and implants, but it cannot detect physiological changes. Magnetic resonance (MR) image provides better information on soft tissue. Medical image fusion aims at integrating information from multimodality medical images to obtain a more complete and accurate description of the same object. It provides an easy access for radiologists to quickly and effectively report CT/MR studies. In fact, in many applications, the medical images obtained from medical instruments are noisy due to imperfection of image capturing devices [3], [4]. Unfortunately, noise is easily mistaken for the useful feature of the image, making the traditional image fusion algorithms invalid, although they can efficiently fuse noise-free images. Thus, it is necessary and challenging to investigate joint fusion and denoising for multimodality medical images.

The goal of image fusion is to automatically transfer the meaningful information contained in multiple source images to a single fused image without introducing information loss. Thus, the study of image fusion has drawn many researchers' attention and is of numerous realistic applications (e.g., people tracking [5] and surface temperature measurement of billets [6]). In the field of medical image fusion, a large number of fusion methods have been proposed [7]–[14]. The purpose of medical image fusion is to extract and synthesize the main features of multimodality images. Therefore, the quality of image fusion highly depends on the performance of image feature extraction. Manchandaa and Sharma [7] used fuzzy transform to extract edge details of multimodal medical images. Du *et al.* [8] first transformed the input images into their multiscale representations by a Laplacian pyramid. Then, they extracted the contrast feature map and outline feature map at each scale, respectively. In [9]–[11], discrete fractional wavelet transform, multiscale discrete wavelet transform, and daubechies complex wavelet transform were sued for extracting detail features, respectively. Liu and Du [12] used the gradient minimization smoothing filter to decompose each source image into one base image and a series of detail images. In [13], nonsubsampled contourlet transform was used to decompose the source medical images into base and edge detail bands. Xu [14] used the local minima and maxima envelopes of the image to extract the features of the source images.

The above methods can produce effective fusion results when the input medical images are noise free. However, if the input medical images are noisy, noise, generally concentrating in high-frequency part of the image, affects the extraction of image details and edge features. Hence, medical image fusion and denoising is a challenging problem.

In order to fuse noisy medical images, an intuitive method is first using technique of image denoising [15]–[17], [18] and

Manuscript received December 11, 2016; revised March 7, 2017; accepted March 12, 2017. This work was supported by the Project funded by China Postdoctoral Science Foundation under Grant 2017M611221 and the National Natural Science Foundation of China under Grant 61528101. The Associate Editor coordinating the review process was Salvatore Baglio. *(Corresponding author: Wenda Zhao.)*

The authors are with the School of Information and Communication Engineering, Dalian University of Technology, Dalian 116024, China (e-mail: zhaowenda@dlut.edu.cn; lhchuan@dlut.edu.cn).

Color versions of one or more of the figures in this paper are available online at http://ieeexplore.ieee.org.

Digital Object Identifier 10.1109/TIM.2017.2700198

then fusing the denoising images. Since denoising smooths the image edges and details, influencing subsequent image feature extraction, this does not obtain good fusion effect. Another method is to average the multimodality images. This can reduce the noise of the fused image, but cannot effectively extract the edge detail information of the input images. In [19], a fusion method was proposed based on maximum *a posteriori* estimate of noisy images, with Gaussian model. This method was further improved in [20] by accounting for non-Gaussianity of the image distributions. In [21], a sparse representation (SR)-based method was proposed. The source image is represented with sparse coefficients using an overcomplete dictionary, by combining the coefficients with the choose-max fusion rule and reconstructing from the combined sparse coefficients and the dictionary to get the fused image. An improved method called dictionary learning with group sparsity and graph regularization was proposed in [22], considering the intrinsic structure. More robust algorithms are based on the wavelet transform algorithms [23], [24]. In particular, Loza *et al.* [24] discussed the use of the generalized Gaussian and alpha-stable distribution for modeling of image wavelet coefficients. It obtained a good effect for the noisy multimodal image fusion, but generated the ringing effect. For image fusion and denoising, another idea is to focus on the effective image denoising algorithms. An impressive approach is using a total variation (TV) model to estimate the pixels of the fused image [25], [26]. The TV model is a data-driven approach and does not require knowledge of the probability density function of the fused pixels, and it can preserve the fused image edge details while suppressing noise. But the TV model is easy to produce the staircase effect [27]. In this paper, a medical image fusion and denoising method with the multiscale alternating sequential filter and adaptive fractional order TV (AFOTV) is proposed. Comparing with the TV-based method [25], [26], the proposed method construct an adaptive fractional order $p(|\nabla u|)$ instead of parameter 1 of TV, which can effectively suppress noise while avoiding the staircase effect. Moreover, the multiscale alternating sequential filter is easily implemented and effective for extracting the features from noisy input medical images. Thus, the proposed method is more robust to noise, which will be verified in Section III. Several advantages of the proposed image fusion approach are highlighted as follows.

1) An effective variation model is proposed to estimate the fused medical image. The proposed fusion framework not only can be used for noisy multimodal medical image fusion, but also can be used for noise-free medical image fusion.
2) A multiscale alternating sequential filter is first innovatively integrated into the multimodal medical image fusion framework by recursive filtering-based weight map technique. It can effectively extract the main characteristics from noisy input medical images, preventing noise interference.
3) TV is developed by constructing an adaptive fractional order $p(|\nabla u|)$ instead of parameter 1, called AFOTV. Through the isotropic diffusion in the flat part of the image and diffusion along the tangential direction of the edge, noise is suppressed while avoiding the staircase effect.

The remainder of this paper is organized as follows. Section II describes the proposed multimodal medical image fusion and denoising method. The experimental results and discussions are presented in Section III. Finally, Section IV concludes this paper.

II. Proposed Method

What we concern here is how to integrate noisy multimodality medical images into an image, where edge details of the input images are preserved with reduced noise. The process of the proposed fusion algorithm is illustrated in Fig. 1. Each step will be introduced in the following contents.

Let $u(x, y)$ be the target fused image, which is obtained from n different sensors and $u_1(x, y), u_2(x, y), \ldots, u_n(x, y)$ are the corresponding n measurement images for $x, y \in \Omega$. The local affine transform between the target fused image and the measured images is defined as [26], [28]

$$u_i(x, y) = w_i(x, y)u(x, y) + n_i^s(x, y), \quad 1 \le i \le n \tag{1}$$

where $w_i(x, y) \in [0, 1]$ and $n_i^s(x, y)$ are the gain and noise of the ith image at location (x, y), respectively. From (1), we have

$$\mathbf{u} = \mathbf{w}u + \mathbf{n^s} \tag{2}$$

where $\mathbf{u} = [u_1, u_2, \ldots, u_n]^T$, $\mathbf{w} = [w_1, w_2, \ldots, w_n]^T$, and $\mathbf{n}^s = [n_1^s, n_2^s, \ldots, n_n^s]^T$. The pixel location (x, y) has been dropped for notational simplicity. Equation (2) can be rearranged as

$$\mathbf{w}^N\mathbf{u} = u + \mathbf{w}^N\mathbf{n^s} \tag{3}$$

where $\mathbf{w}^N = (\mathbf{w}^T\mathbf{w})^{-1}\mathbf{w}^T$.

The goal of fusion is to integrate noisy multimodal medical image into one image that preserves details (i.e., dense structures, soft tissue and blood flow) of the input images while reducing noise. For joint fusion and denoising, we propose the variation model as follows:

$$E(u) = \min \iint_\Omega (u - \mathbf{w}^T\mathbf{u})^2 dxdy + \lambda \iint_\Omega |\nabla u|^{p(|\nabla u|)} dxdy \tag{4}$$

where $\mathbf{w} = [w_1, w_2, \ldots, w_n]^T$, $w_n \in [0, 1]$ being the weight function corresponding the source image u_n, satisfying $\sum_{i=1}^n w_i = 1$, $0 < \lambda < 1$ is a scalar of tradeoff between the fidelity and the smoothness of the fused image, $|\nabla u|$ is the gradient amplitude of the image u, $|\nabla u|^{p(|\nabla u|)}$ represents the AFOTV, and $p(|\nabla u|)$ is taken different values adaptively according to the different local information of the image u. In (4), the first term serves for image fusion and is called the fusion term, and the second term plays the role of image denoising and is called the regularity term.

To solve the variation (4), we use the gradient descendent method [25]. Its Euler–Lagrange equation is

$$u - \mathbf{w}^T\mathbf{u} - \lambda\nabla \cdot \left[q(|\nabla u|)\frac{\nabla u}{|\nabla u|} \right] = 0 \tag{5}$$

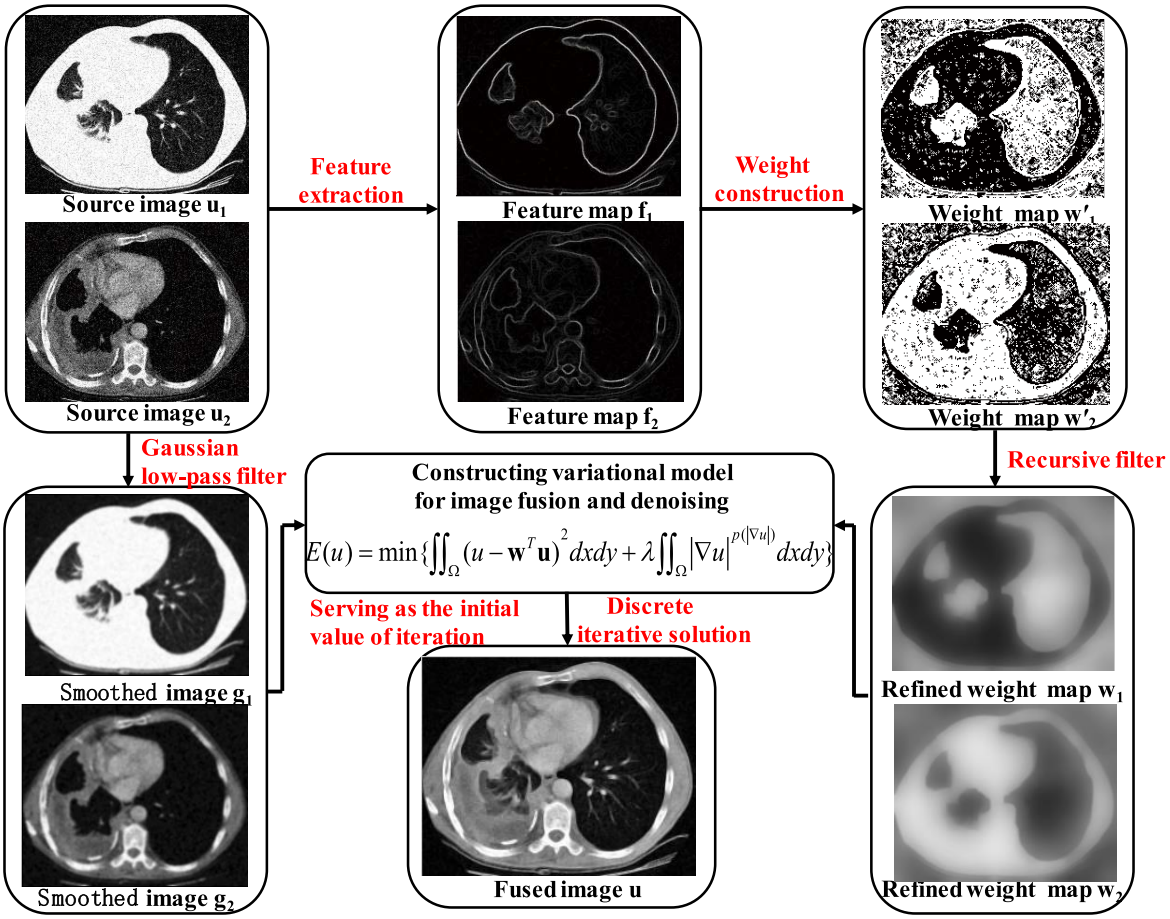

Fig. 1. Flowchart of the proposed medical image fusion and denoising framework.

where "·" represents the dot product and $q(|\nabla u|) = p(|\nabla u|)|\nabla u|^{p|\nabla u|-1} + (ln|\nabla u|)p\prime(|\nabla u|)|\nabla u|^{p(|\nabla u|)}$. Then, (5) can be embedded into the evolution with the time step τ like (6). To ensure the convergence, τ should be a small positive value

$$\frac{\partial u}{\partial \tau} = \mathbf{w}^T\mathbf{u} - u + \lambda\nabla\cdot\left[q(|\nabla u|)\frac{\nabla u}{|\nabla u|}\right]. \tag{6}$$

Using the time-forward difference scheme, minimization of the solution of (4) can be achieved iteratively

$$u^{(n+1)} = u^n + \tau\left\{\mathbf{w}^T\mathbf{u} - u^n + \lambda\nabla\cdot\left[q(|\nabla u^n|)\frac{\nabla u^n}{|\nabla u^n|}\right]\right\} \tag{7}$$

where n represents the number of iterations.

Next, the issue is how to construct the weight function w_n and the adaptive fractional order $p(|\nabla u|)$. The weight function should highlight the main features of the source image without interference by noise. It consists two parts: feature extraction and weight construction, which will be introduced in Sections II-A and II-B, respectively. In order to suppress noise and do not produce the staircase effect, $p(|\nabla u|)$ should take different values adaptively to make the isotropic diffusion in the flat part of the image and diffusion along the tangential direction of the edge, and this will be introduced in Section II-C. Once the weight function w_n and the adaptive fractional order $p(|\nabla u|)$ are obtained, the proposed algorithm is then applied for multimodal medical image fusion and denoising.

A. Feature Extraction With Multiscale Alternating Sequence Filter

Medical images often contain different levels of noise. Unfortunately, noise and features of the image have similar characteristics in the spatial and frequency domains, making it difficult to image feature extraction. Here, an image feature extraction method based on a morphological multiscale alternating sequence filter is proposed.

Mathematic morphology is a nonlinear image processing based on set theory, and it has been applied to image processing widely [29], [30]. Morphological operation has been successfully applied for edge detection [31], [32]. The basic operations of mathematical morphology are dilation, erosion, opening, and closing, which are defined as follows. Let $f(x, y)$ and $B(u, v)$ represent the input image and plat structuring element, respectively. The basic morphological operations are dilation and erosion, denoted by $f \oplus B$ and $f \ominus B$, which are defined as follows:

$$f \oplus B = \max_{u,v}(f(x-u, y-v) + B(u, v)) \tag{8}$$

$$f \ominus B = \min_{u,v}(f(x+u, y+v) - B(u, v)). \tag{9}$$

In mathematical morphology, dilation can merge the points of the background image into the surrounding objects, and

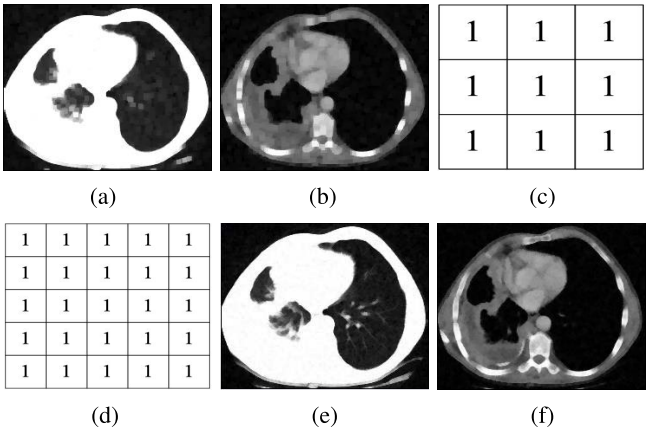

Fig. 2. (a) and (b) Filter results using (c) and (d) traditional structuring elements, which are for the closing and opening operations, respectively. (e) and (f) Filter results using the proposed method.

erosion can eliminate the boundary points of the object [33]. Other two important operations, which are opening and closing and denoted by $f \circ B$ and $f \bullet B$, are defined as follows:

$$f \circ B = (f \ominus B) \oplus B \tag{10}$$

$$f \bullet B = (f \oplus B) \ominus B. \tag{11}$$

Closing can remove the small holes and fill the gaps on the contour, while opening can eliminate the "glitches" and scatters of the object edge. Thus, by alternately operating the closing and opening, the alternating sequence filter can be realized, which is defined as follows [34], [35]:

$$\mathrm{ASF}_k = \alpha_k \beta_k \alpha_{k-1} \beta_{k-1} \ldots \alpha_1 \beta_1 \tag{12}$$

where α_k and β_k represent the closing and opening operations, respectively. In this paper, $A(f)$ is used to represent the alternating sequence filter operation, where f is the input image.

The shape and size of the structuring element are two important parameters used in the alternating sequence filter. Using a traditional structuring element, the alternating sequence filter easily oversmooths edge details, as shown in Fig. 2(a) and (b). The original noisy images are shown in Fig. 1.

In general, the shape of the structuring element should be similar to object boundary, and this can reduce noise while preserving the object boundary. In this paper, we assume that various boundaries can be constituted by a series of horizontal, vertical, or inclined lines. And the four different directions are selected: 0°, 45°, 90°, and 135°. We use the structuring element of 3×3 for closing operation to reduce noise and the structuring and the structuring element of 5×5 for opening operation to fill the holes generated by closing operations. The structuring elements are shown in Figs. 3 and 4.

Then, we redefine α_k and β_k

$$\alpha_k = \frac{1}{4} \sum_{j=0^\circ}^{135^\circ} \alpha_k^j, \quad \beta_k = \frac{1}{4} \sum_{j=0^\circ}^{135^\circ} \beta_k^j \quad \{j | j = 0^\circ, 45^\circ, 90^\circ \text{ and } 135^\circ\} \tag{13}$$

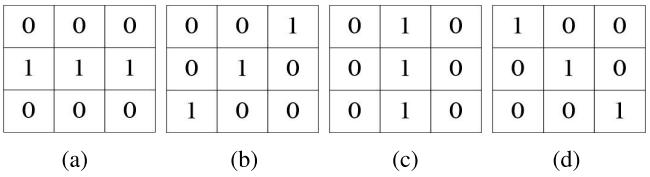

Fig. 3. Structuring element of 3×3. (a)–(d) Structuring element in 0°, 45°, 90°, and 135° directions, which are expressed as $B_{3\times3}^{0^\circ}$, $B_{3\times3}^{45^\circ}$, $B_{3\times3}^{90^\circ}$, and $B_{3\times3}^{135^\circ}$, respectively.

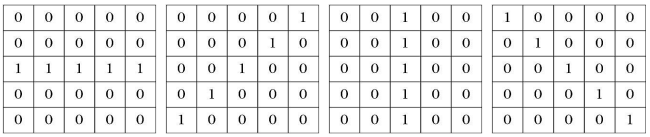

Fig. 4. Structuring element of 5×5. (a)–(d) Structuring element in 0°, 45°, 90°, and 135° directions, which are expressed as $B_{5\times5}^{0^\circ}$, $B_{5\times5}^{45^\circ}$, $B_{5\times5}^{90^\circ}$, and $B_{5\times5}^{135^\circ}$, respectively.

where α_k^j and β_k^j represent the closing and opening operations in the j direction, respectively. Using the redefined α_k and β_k for the alternating sequence filter, the results are shown in Fig. 2(e) and (f). Noise is effectively suppressed while preserving image edge details.

Based on the above multiscale alternating sequence filter $A(f)$, we define the image feature extraction method as follows:

$$F(u_i) = (u_i \oplus B_{3\times3}) \oplus B_{5\times5} - A(u_i) \tag{14}$$

where $F(u_i)$ is the image feature of the input image u_i, and $B_{3\times3}$ and $B_{5\times5}$ are defined as

$$B_{3\times3} = \frac{1}{4} \sum_{j=0^\circ}^{135^\circ} B_{3\times3}^j, \quad B_{5\times5} = \frac{1}{4} \sum_{j=0^\circ}^{135^\circ} B_{5\times5}^j \quad \{j | j = 0^\circ, 45^\circ, 90^\circ \text{ and } 135^\circ\}. \tag{15}$$

As shown in Fig. 1, the proposed image feature extraction method can effectively extract the main features from the noisy source image.

B. Construction of Weight w_n With Recursive Filter

The weight should highlight the main feature from the source images, so the feature maps are compared to determine the weight map as follows:

$$w_n'(x, y) = \begin{cases} 1 & F_n(x, y) = \underbrace{F_1(x, y), F_2(x, y), \ldots, F_N(x, y)}_{\max} \\ 0 & \text{otherwise} \end{cases} \tag{16}$$

where N is the number of source images, $F_n(x, y)$ is the feature value of the pixel (x, y) in the nth image. As shown in Fig. 1, the weights estimated above are noisy and hard (0 or 1), which may produce artifacts to the fused image. In [36], guided filtering (GF) was applied for weight refinement and the source image was adopted as the reference image

for GF. However, in this paper, the source image is noisy, and if it is used as the reference image for GF, the effect of smoothing weight map will be greatly reduced. Thus, we use the recursive filter to smooth the weight map, and it is defined as follows [13], [37]:

$$J[k] = (1 - a^d)I(k) + a^d J[k-1] \tag{17}$$

where $a \in [0, 1]$ represents a feedback coefficient, $I(k)$ represents the value of the pixel of the kth input weight map, $J[k]$ is the value of the kth pixel of the refined weight map, and d is the distance between neighborhood pixels of the source medical image. a^d goes to zero as d increases and the propagation chain will stop. Thus, pixels with similar gray values tend to have similar smoothed weight. Here, the recursive filter is performed on the weight map w'_n

$$\widetilde{w}_n = \mathrm{RF}_{\sigma_s,\sigma_r}\left(w'_n\right) \tag{18}$$

where RF denotes the recursive filter operation, and σ_s and σ_r the parameters and they, respectively, control the space and range support of the recursive filter [13]. Then, $\widetilde{w}_n$ is normalized as follows:

$$w_n = \left(\sum_{i=1}^{n} \widetilde{w}_i\right)^{-1} \widetilde{w}_n. \tag{19}$$

As shown in Fig. 1, the redefined weight maps can transform the hard and noise weight maps into smooth weight maps and can well highlight the main features in each source medical image.

C. Estimation of Adaptive Fractional Order $p(|\nabla u|)$

The TV model has been widely applied to image processing [25], [26], [38]. It can suppress noise while preserving the image edge details. But it is easy to produce the staircase effect in the smooth region [27]. In [39], the fractional order is taken as 2. This model effectively keeps the image smooth area, but blurs the image edge. In this paper, AFOTV constraint is constructed for image denoising and the model is shown in (4). According to characteristics of the image, $p(|\nabla u|)$ adaptively takes different values to suppress noise while preserving the image edge and does not produce the staircase effect. Here, $p(|\nabla u|)$ is structured as

$$p(|\nabla u|) = 1 + e^{-\frac{|\nabla u|}{\mathrm{aver}(|\nabla u|)}} \tag{20}$$

where aver$(|\nabla u|)$ is the average value of the gradient $|\nabla u|$, reflecting the attenuation rate of the fractional order $p(|\nabla u|)$ with the increase in the gradient aver$(|\nabla u|)$. As is shown in Fig. 5 (a), with the increase in aver$(|\nabla u|)$, the attenuation rate of $p(|\nabla u|)$ flattens. At the image detail edge, the gradient $|\nabla u|$ is large. Then, based on (20), $p(|\nabla u|)$ is small, which is approximately equal to 1, as shown in Fig. 5(a) (see the bold red dotted line) and (b). Fig. 5(b) shows the gradient histogram of the image in Fig. 5(c), intuitively reflecting the distribution of image gradient. And the image detail edges correspond to large gradients in Fig. 5(b). The bold red curve of Fig. 5(a) is structured based on aver$(|\nabla u|)$ of Fig. 5(c). Therefore, along the edge direction, it has a large diffusion, and in the vertical direction of the edge, it has a very small diffusion, and this keeps the image detail edge. At the plat region of the image, the gradient $|\nabla u|$ is small. Based on (20), $p(|\nabla u|)$ is large, which is approximately equal to 2, as shown in Fig. 5(a) (see the bold red dotted line) and (b). Therefore, in all directions it has isotropic diffusion, and this avoids the staircase effect. From Fig. 5(c), the proposed approach can effectively extract and fuse the main feature from noisy input images. Then, after adding the AFOTV constraint, the proposed approach effectively suppresses noise, as shown in Fig. 5(d).

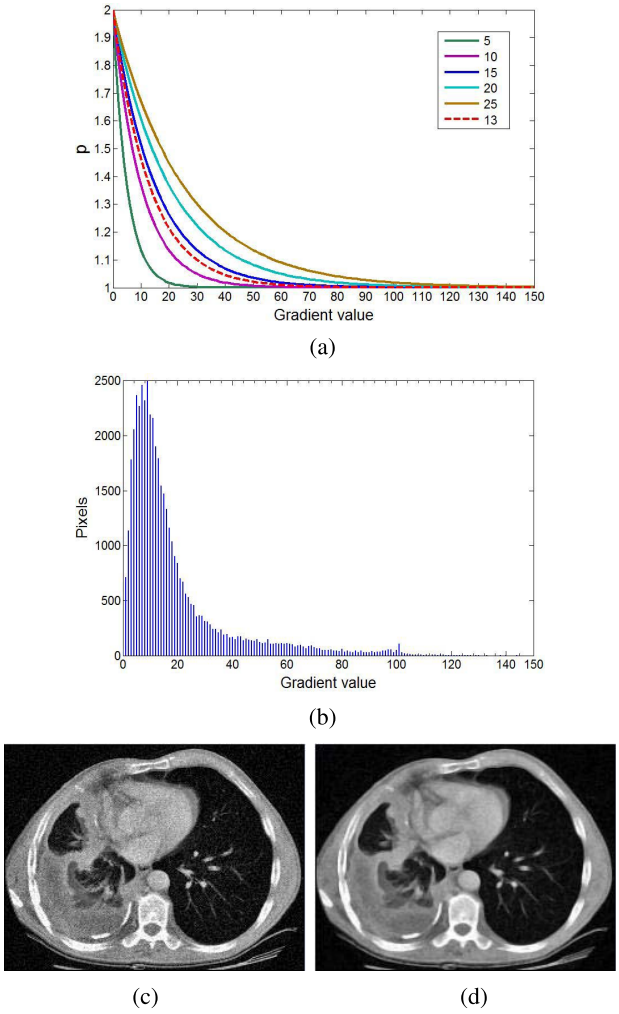

(a) (b) (c) (d)

Fig. 5. (a) Graph of $p(|\nabla u|)$ corresponding to different values of $aver(|\nabla u|)$. (b) Gradient histogram of the image in (c). (c) Fused image by the proposed approach without the AFOTV constraint. (d) Fused image by the proposed approach.

III. Experiments and Discussion

A. Objective Image Fusion Quality Metrics

In order to assess the fusion performance of different methods objectively, five fusion quality metrics are adopted [40]–[42], which would be introduced as follows.

1) *Signal-to-Noise Ratio:* The signal-to-noise ratio is given by

$$\mathrm{SNR} = 10\log_{10}\left[\frac{\sum_{i=1}^{X}\sum_{j=1}^{Y}(R_{ij})^2}{\sum_{i=1}^{X}\sum_{j=1}^{Y}(R_{ij} - F_{ij})^2}\right] \tag{21}$$

where X and Y denote the number of rows and columns of the image, respectively, and R_{ij} and F_{ij} denote the pixel value in (i, j) of the reference image and fused image, respectively. A high SNR value indicates that the reference and fused images are similar. For noisy image fusion, higher value indicates better performance of fusion and denoising.

2) *Root-Mean-Square Error:* The root-mean-square error is given by

$$\text{RMSE} = \sqrt{\frac{\sum_{i=1}^{X}\sum_{j=1}^{Y}(R_{ij} - F_{ij})^2}{X \times Y}}. \tag{22}$$

The RMSE value will increase when the similarity between the reference and fused images decreases. Then, a smaller RMSE value stands for better fusion.

3) *Correlation:* The correlation is given by

$$\text{CORR} = \frac{2C_{rf}}{C_r + C_f} \tag{23}$$

where $C_r = \sum_{i=1}^{X}\sum_{j=1}^{Y}(R_{ij})^2$, $C_f = \sum_{i=1}^{X}\sum_{j=1}^{Y}(F_{ij})^2$ and $C_{rf} = \sum_{i=1}^{X}\sum_{j=1}^{Y}(R_{ij})(F_{ij})$. The CORR value is closer to 1 when the reference and fused images are more similar.

4) *Entropy:* The entropy is given by

$$\text{En} = -\sum_{i=0}^{L-1} p_i \log p_i \tag{24}$$

where p_i stands for the ratio of the pixel number N_i of the gray value i and the total pixel number N, which is expressed as

$$p_i = \frac{N_i}{N}, \quad 1 \le i \le L-1. \tag{25}$$

En is used for the no-reference image fusion quality metric. A larger En value means the fused image contains more information. Thus, the corresponding fusion approach has the better performance.

5) *Gradient-Based Index:* The gradient-based index is given by

$$\text{QG} = \frac{\sum_{i=1}^{X}\sum_{j=1}^{Y}(Q^{AF}(i,j)\tau^{A}(i,j) + Q^{BF}(i,j)\tau^{B}(i,j))}{\sum_{i=1}^{X}\sum_{j=1}^{Y}(\tau^{A}(i,j) + \tau^{B}(i,j))} \tag{26}$$

where $Q^{AF} = Q_g^{AF} Q_o^{AF}$, $Q_g^{AF}(i, j)$ and $Q_o^{AF}(i, j)$ are the edge strength and orientation preservation values at location (i, j), respectively, and $Q_{BF}(i, j)$ is similar to $Q_{AF}(i, j)$. $\tau^A(i, j)$ and $\tau^B(i, j)$ reflect the importance of $Q_{AF}(i, j)$ and $Q_{BF}(i, j)$, respectively. QG is used for the no-reference image fusion quality metric. The value of QG is within the range [0, 1], and a higher value indicates a better fusion result.

B. Experimental Setup

The proposed algorithm is applied to different multimodal medical images available online in [44] and [45]. Since images available in [44] and [45] are registered, no image registration technique is applied to these images prior to fusion. Experiments are set from three aspects to verify the performance of the proposed algorithm. First, the medical images are added by computer-generated zero-mean Gaussian white noise and noise levels are measured using signal-to-noise ratio (SNR), and several different levels of SNR are used to validate the robustness to noise of the proposed algorithm. Then, comparing with SR-based fusion [21], non-Gaussian model-based fusion of noisy images in the wavelet domain (NGWT) [24], TV based for pixel-level image fusion (TVPL) algorithm [26], and a combination method block matching and 3-D filtering+guided filtering fusion (BM3D+GFF), which first uses BM3D [45] to remove noise and then the state-of-the-art fusion method (GFF) [36], experiments are performed on different noisy multimodal medical images to verify the performance of fusion and denoising of the proposed algorithm. Finally, comparing with simple averaging (AVG), SR [21], and wavelet-based transform [discrete wavelet transform (DWT) with DBSS (2,2)] [46], experiments are performed on different noise-free multimodal medical images to verify the performance of fusion of the proposed algorithm. The parameter settings of these methods are as follows. There are four decomposition levels, in which the "averaging" scheme is for the low-pass sub-band and the absolute maximum choosing scheme is for the bandpass sub-band. Experiments are performed on different medical images, and typical five pairs of multimodal medical images are selected in this paper to verify the effectiveness of the proposed algorithm. Fig. 6 shows the multimodal database. The referenced fusion images are obtained by the fusion method in [36]. The

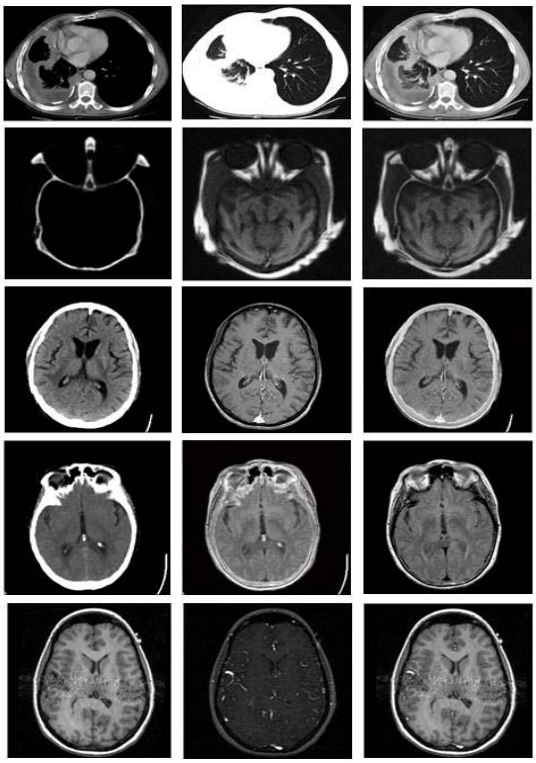

Fig. 6. Image database composed of five pairs of multimodal medical images. First and second columns: source images, respectively. Third row: corresponding referenced fusion images obtained by the fusion method in [36], respectively.

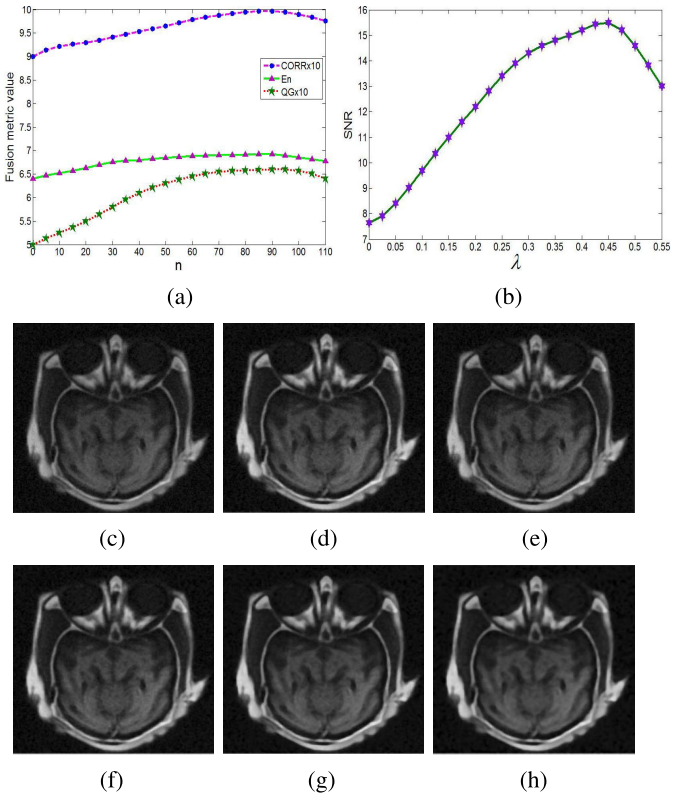

Fig. 7. Performance of the proposed method with different parameters. (a) Graphical representation of the fusion metric value of CORR, En, and QG when $\lambda = 0.35$ and n is taken different values. (b) Graphical representation of the fusion metric value of SNR when $n = 90$ and λ is taken different values. (c)–(e) Fusion results when $\lambda = 0.35$ and n takes 60, 90, and 100, respectively. (f)–(h) Fusion results when $n = 90$ and λ takes 0.4, 0.45, and 0.5, respectively.

method in [36] has state-of-the-art performance for fusion of clear multimodal images. Therefore, the referenced fusion images well preserve the complementary information of multimodal input images, as shown in the third column of Fig. 6.

In the proposed method, k in (12) represents the number of alternating sequences. The parameter k is introduced to adjust the degree of noise suppression and edge detail protection. If k is too large, noise can be effectively suppressed but edge details is oversmoothed. This directly affects the image feature extraction. $k = 2$ can obtain good results for most images. In (18), the parameters σ_s and σ_r, respectively, control the space and range support of the recursive filter. They directly affect the smooth degree of the weight maps. Here, $\sigma_s = 100$ and $\sigma_r = 4$ are set as the default parameters. The detailed description of rational for selecting σ_s and σ_r can be found in [13]. λ in (4) is a scalar of tradeoff between the fidelity and the smoothness of the fused image. The number of iterations n in (7) is an adjustable parameter, making the result tend to the optimal solution in different degrees. Fig. 7 presents objective evaluations of the results obtained by the proposed method with different n and λ.

Fig. 7(a) shows the performance of the proposed method when n is taken different values and λ is taken a fixed value of 0.35. The fusion metric value of CORR, En, and QG gradually increases as n increases, until reaching their maximum values, respectively. After $n = 90$, their values decrease gradually. Fig. 7(c)–(e) visually illustrates this influence that the fused image in Fig. 7(d) has a better reconstruction effect than those in Fig. 7(c) and (e). This phenomenon indicates that we can find the optimum result through limited iterations. To obviously show the change of CORR and QG values, they are multiplied by 10 in Fig. 7(a), and this does not affect the analysis of the parameter n. Fig. 7(b) shows the performance of the proposed method when λ is taken different values and n is taken a fixed value of 90. As λ increases, the value of SNR gradually increases, illustrating that the ability of denoising of the proposed method is enhanced. After $\lambda = 0.45$, the value of SNR decreases gradually. And the reason is that the fusion image is oversmoothed. Fig. 7(f)–(h) visually illustrates this influence of λ. Comprehensively considering the detail preservation and noise suppression, we take $\lambda = 0.45$ and $n = 90$.

TABLE I

QUALITY MEASURES TO EVALUATE THE CAPABILITY OF THE FUSION AND DENOISING USING SNR

	Proposed method without AFOTV	Proposed method
Input images added 10.56 dB SNR	11.26	19.90
Input images added 7.85 dB SNR	8.78	16.18
Input images added 5.09 dB SNR	7.32	13.57

C. Experimental Results and Discussion

1) Robustness of the Proposed Method to Noise: Three sets of fusion results for the 10.56-, 7.85-, and 5.09-dB SNRs have been presented in Fig. 8 to validate the robustness to noise of the proposed algorithm. Fig. 8(a) and (b) shows the images of a human brain obtained using CT and MR imaging (MRI), respectively. CT and MRI sensors provide complementary information, where the CT image shows the bones, whereas the MRI image displays the soft tissue information. From Fig. 8(d), it can be confirmed that the fused images look more pleasing compared with the noisy input images. For high level of SNR [see the second row or the third row in Fig. 8(a) and (b)], the proposed approach can effectively extract and fuse the main feature (i.e., bone and soft tissues) from noisy input images, as shown in Fig. 8(c). Then, after adding the AFOTV constraint, the proposed approach effectively suppresses noise and the fused image has clear details and good visual effects [see Fig. 8(d)]. Table I shows the quality measures to evaluate the capability of the fusion and denoising of the proposed approach. The SNR of fused image by the proposed approach without AFOTV is higher than that of the noisy input images, demonstrating that the weight construction based on the multiscale alternating sequential filter in this paper can effectively extract the detail and edge features from the noisy input images. And after adding AFOTV, the SNR is about double, indicating good performance of the proposed algorithm for noise suppression.

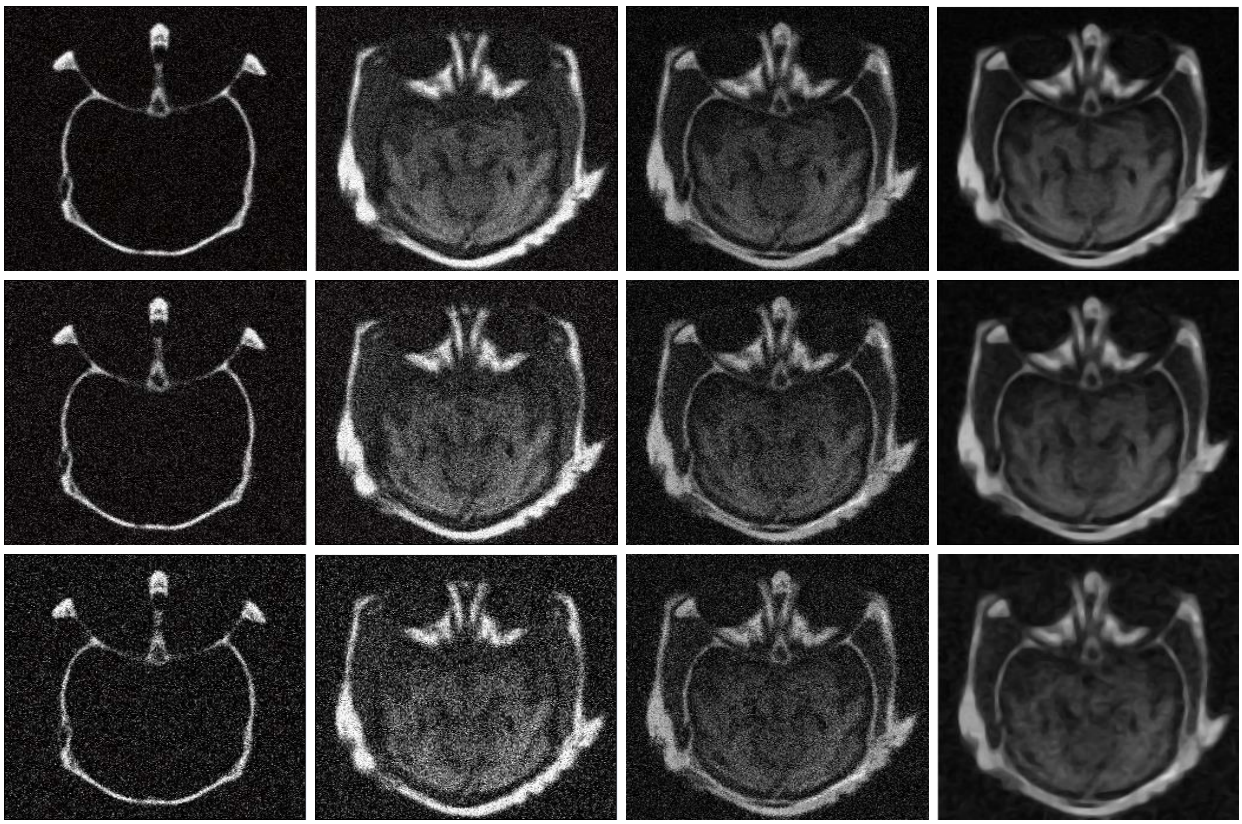

Fig. 8. Medical image fusion with different levels of SNR. (a) and (b) First row to third row: noisy input images that are added 10.56-, 7.85-, and 5.09-dB SNRs, respectively. (c) Fused images by the proposed approach without AFOTVC. (d) Fused images by the proposed method.

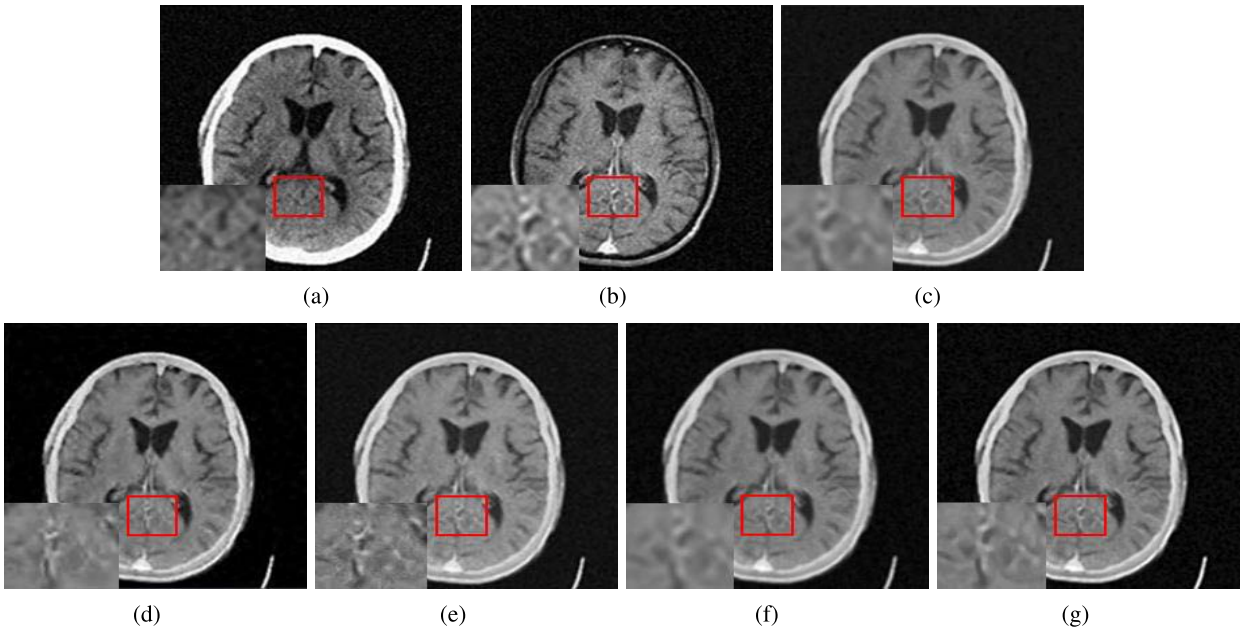

Fig. 9. Input images that are added a 13.48-dB SNR and fusion result comparison with different methods. (a) Noisy CT image. (b) Noisy MR image. (c) SR. (d) NGWT. (e) TVPL. (f) BM3D + GFF. (g) Proposed method.

2) Comparison With Other Image Fusion Methods for Noisy Input Images: Fig. 9(a) and (b) shows two medical images: CT and MR images that are added noise of 13.475-dB SNR. The CT image shows the calcification and the MR image reveals several focal lesions involving basal ganglia with some surrounding edema, respectively. Fig. 10(a) and (b) shows CT

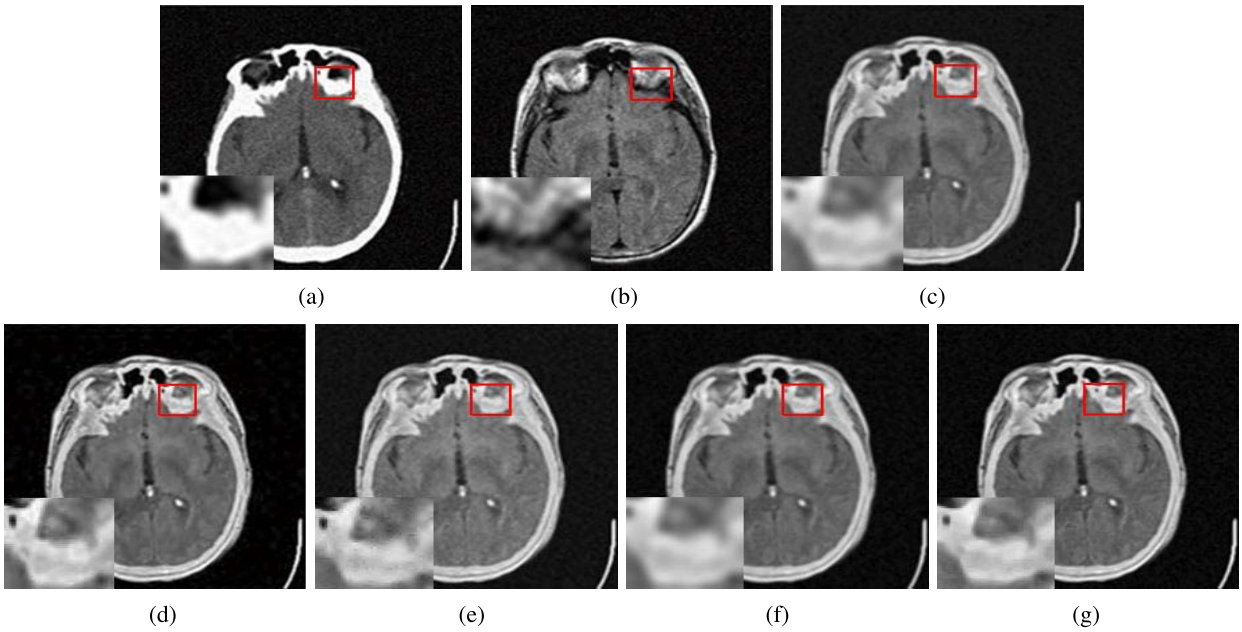

Fig. 10. Input images that are added an 11.51-dB SNR and fusion result comparison with different methods. (a) Noisy CT image. (b) Noisy PD image. (c) SR. (d) NGWT. (e) TVPL. (f) BM3D + GFF. (g) Proposed method.

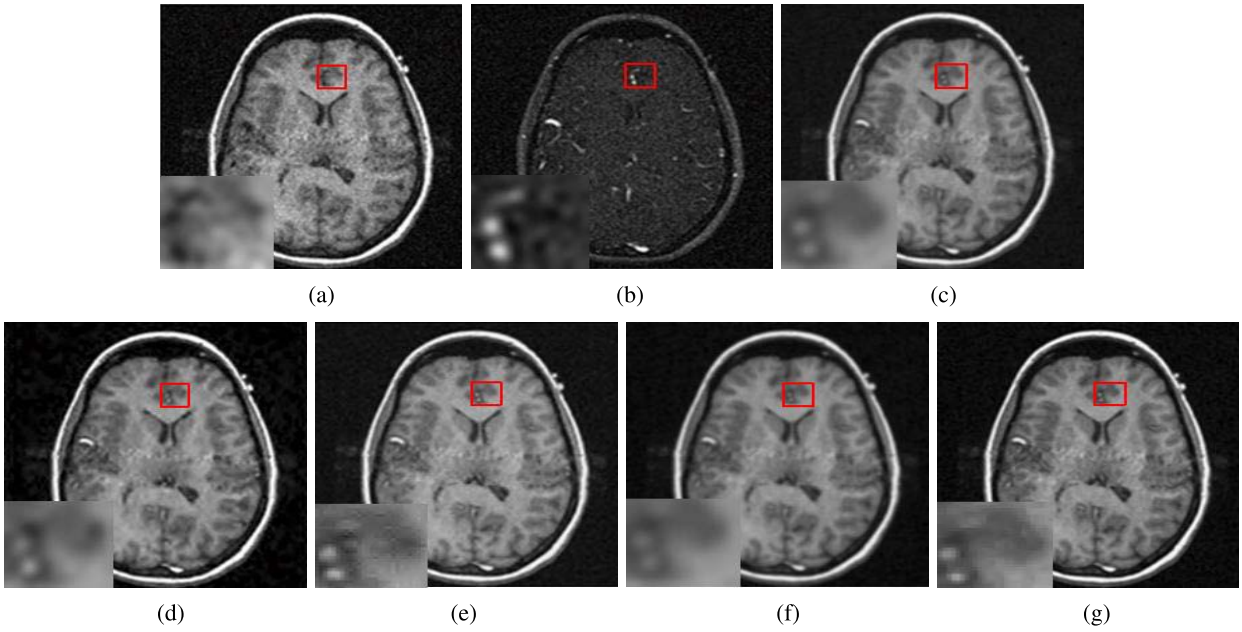

Fig. 11. Input images that are added a 4.12-dB SNR and fusion result comparison with different methods. (a) Noisy T1-MR image. (b) Noisy MRA image. (c) SR. (d) NGWT. (e) TVPL. (f) BM3D+GFF. (g) Proposed method.

and proton density (PD) weighted MR images that are added an 11.506-dB SNR, respectively. The CT image indicates a medial left occipital infarct involving the left side of the splenium of the corpus callosum and the PD weighted MR image reveals only mild narrowing of the left posterior cerebral artery. T1-weighted MR and MRA images that are added a 4.156-dB SNR are shown in Fig. 11(a) and (b), respectively. The T1-weighted MR image contains the soft tissues and a lesion in the brain, whereas MRA displays the vascular nature of the lesion. In Figs. 9(c)–11(c), SR effectively suppresses noise, but edge details of the fused image are smoothed. From Fig. 9(d)–11(d), it can be seen that the results produced by the NGWT method oversmooths some visually important features, and thus make some details unclear such as the focal lesions and soft tissues. As shown in Figs. 9(e)–11(e), the TVPL-based method keeps the edge details of the input images, but produces the staircase effect, making the fused image have bad visual effect. In Figs. 9(f)–11(f), since BM3D removes noise but smooths details, BM3D+GFF effectively suppresses noise, but edge details of the fused images are

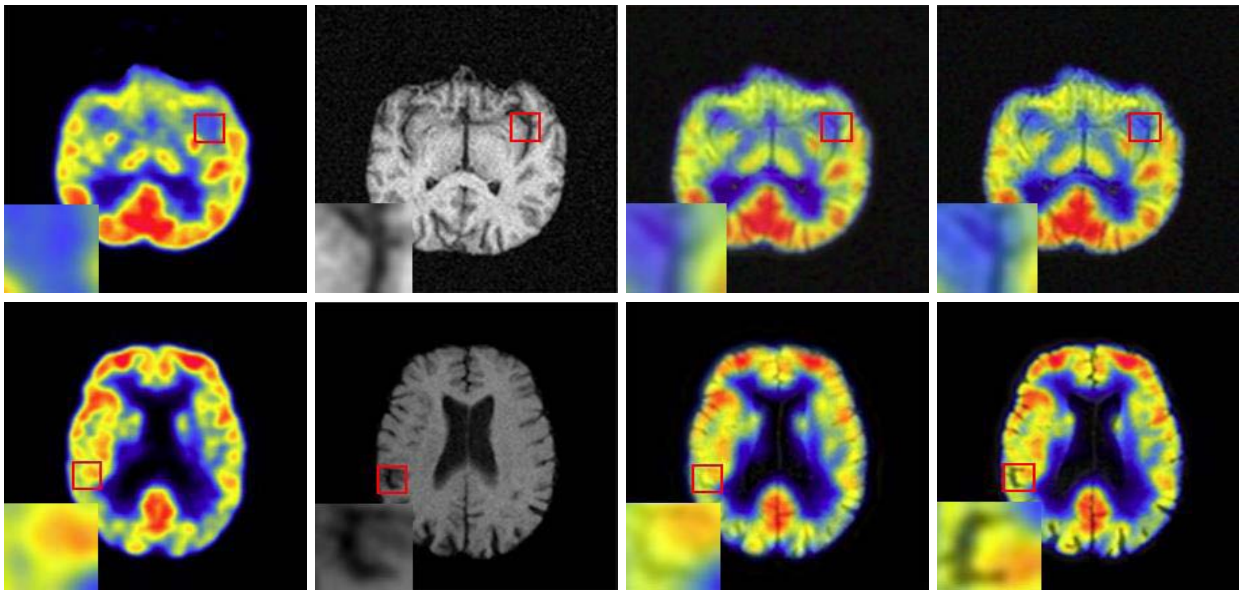

(a) (b) (c) (d)

Fig. 12. Experimental comparison of PET and MRI image fusion. (a) PET image. (b) MRI image. (c) SR. (d) Proposed method.

TABLE II

QUANTITATIVE ASSESSMENT OF DIFFERENT IMAGE FUSION METHODS FOR NOISY IMAGE FUSION. THE BEST TWO RESULTS ARE SHOWN IN RED AND BLUE FONTS

	Index	SR	NGMF	TVPL	BM3D +GFF	Proposed method
Fig. 9	En	6.51	6.19	6.62	6.54	6.77
	SNR	23.86	22.25	21.02	23.64	24.84
	RMSE	23.88	20.39	23.10	24.20	18.23
	CORR	0.97	0.98	0.97	0.97	0.99
	QG	0.61	0.56	0.54	0.56	0.64
Fig. 10	En	6.68	6.67	6.62	6.74	6.83
	SNR	22.96	14.55	21.96	16.89	24.42
	RMSE	31.18	35.76	35.01	33.16	30.97
	CORR	0.96	0.93	0.95	0.95	0.96
	QG	0.63	0.57	0.61	0.59	0.66
Fig. 11	En	6.85	7.15	7.02	6.91	7.20
	SNR	20.47	21.70	14.57	15.69	22.80
	RMSE	24.54	23.69	28.67	28.59	21.42
	CORR	0.97	0.97	0.96	0.97	0.98
	QG	0.51	0.53	0.54	0.49	0.56

fuzzy. In contrast, the proposed method can preserve these features and details without producing the staircase effect, and the fused images have the clearest edge details, as shown in Figs. 9(g)–11(g). The quantitative evaluations of different image fusion methods are given in Table II. The "red" values indicate the best performance for visually convincing tradeoff between noise reduction and detail information loss. From Table II, we can see that the quantitative evaluations of the fused images obtained by the proposed method are the best.

Fig. 12 shows two sets of medical images: PET and MRI images, which are available online in [41]. Fig. 12(b) shows a real MRI image, containing some noise. We use HIS transform to fuse color images [47]. In Fig. 12(c), SR effectively suppresses noise, but loses some anatomical contours shown in the enlarged red rectangle. However, the structures such as the anatomical contours and cerebellar vermis are nicely distinguishable in the proposed method, and the fused images have better visual effect, as shown in Fig. 12(d).

3) Comparison With Other Image Fusion Methods for Noise-Free Input Images: Fig. 13 shows three pairs of noise-free multimodal medical and the fused images obtained by different methods. As shown in Fig. 13(f), the fused image obtained by the proposed method can well preserve the complementary information of the different source. From Fig. 13(c) and (d), it can be seen that the results produced by the AVG and SR methods may decrease the contrast of soft-tissue structures, and thus make some details invisible. As shown in Fig. 13(e), the DWT-with-DBSS-based method improves the contrast of details such as bones and soft-tissue structures, but introduces serious artifacts to the fused image. The quantitative evaluations of different image fusion methods are given in Table III. It is demonstrated from Table III that a better fusion performance can be achieved by the proposed method.

4) Computational Complexity Analysis: Here, experiments are performed using MATLAB on a CPU 2.5-GHz PC with a 2-GB memory. The computational cost of the proposed method is mainly determined by two parts: 1) the multiscale alternating sequential filter for extracting the useful features and 2) recursive-filtering-based weight map technique for fusing the features and iteratively solving the variation model in (4). The complexity of the multiscale alternating sequential filter is $O(2kN)$, where k is the number of alternating sequences and N is the number of pixels. The complexity of the recursive filter is $O(N)$. The most time-consuming part of the proposed

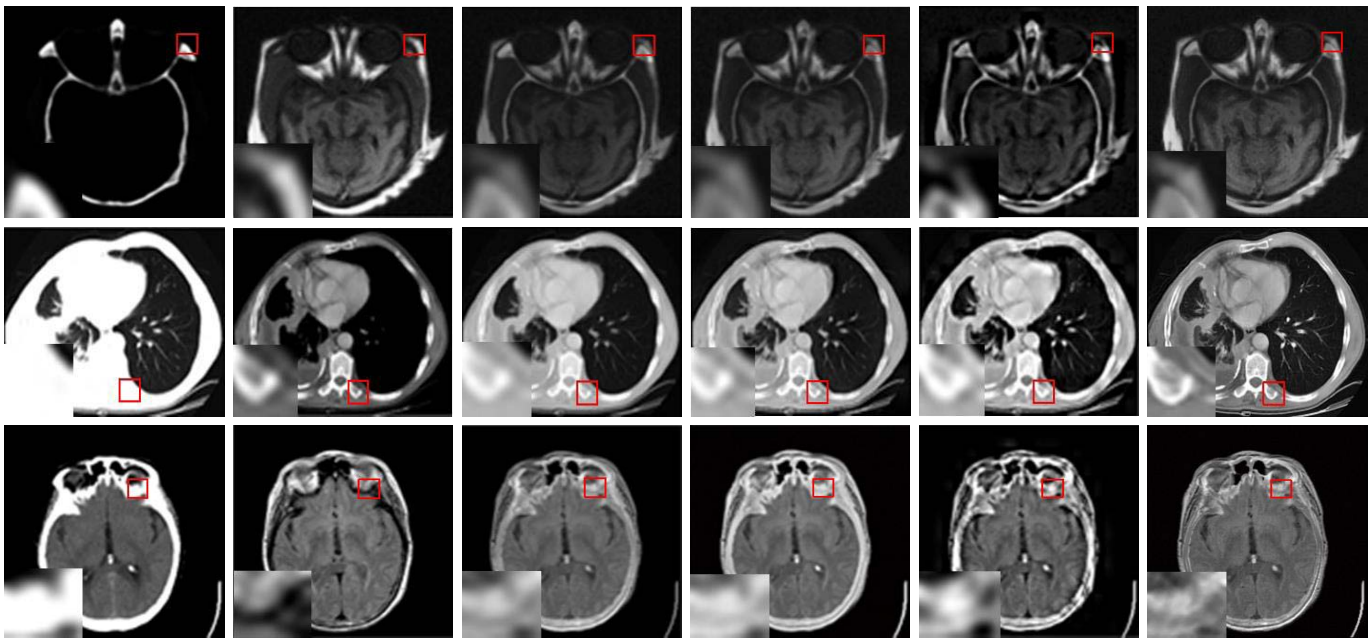

(a) (b) (c) (d) (e) (f)

Fig. 13. Noise-free input images and the fused images obtained by different methods. (a) Input image 1. (b) Input image 2. (c) AVG. (d) SR. (e) DWT with DBSS. (f) Proposed method.

TABLE III

QUANTITATIVE ASSESSMENT OF DIFFERENT IMAGE FUSION METHODS FOR NOISE-FREE IMAGE FUSION. THE BEST TWO RESULTS ARE SHOWN IN RED AND BLUE FONTS

	Index	AVG	SR	DWT with DBSS	Proposed method
First row	En	5.91	6.34	6.12	6.45
	SNR	7.29	8.10	7.20	16.04
	RMSE	32.59	29.70	32.94	11.90
	CORR	0.35	0.40	0.38	0.99
	QG	0.54	0.74	0.67	0.80
Second row	En	6.82	7.01	6.48	7.13
	SNR	14.44	15.16	13.64	16.93
	RMSE	23.55	21.66	25.82	17.68
	CORR	0.50	0.50	0.51	0.99
	QG	0.49	0.72	0.69	0.83
Third row	En	4.41	5.44	5.25	5.57
	SNR	13.37	12.75	10.18	15.71
	RMSE	19.99	21.47	28.89	15.28
	CORR	0.45	0.46	0.46	0.99
	QG	0.56	0.77	0.66	0.81

method is iteratively solving the variation model and its complexity is $O(nN)$, where n is the number of iterations. The consuming time of the proposed method for processing the images of size 344×344 is 9.45 s. Therefore, the future work is to solve the variation model using a more efficient method.

IV. CONCLUSION

A novel and effective variation-model-based method for multimodal medical image fusion and denoising has been presented. The multiscale alternating sequential filter is first innovatively integrated into the multimodal medical image fusion framework by recursive filtering-based weight map technique. It can effectively extract the main characteristics from noisy input medical images, preventing noise interference. Furthermore, the local AFOTV constraint is constructed to further suppress noise, overcoming the shortcoming of the TV. The experiments demonstrate that the proposed method provides a more general solution and is successfully applied to the fusion of noisy and noise-free multimodal medical images. Encouragingly, the proposed method can greatly suppress noise while well preserving the complementary information and main features of noisy input medical images. Future research will be done for the adaptability of the parameters.

REFERENCES

[1] Y. Yang, Y. Que, S. Huang, and P. Lin, "Multimodal sensor medical image fusion based on type-2 fuzzy logic in NSCT domain," *IEEE Sensors J.*, vol. 16, no. 10, pp. 3735–3745, May 2016.

[2] R. Srivastava, O. Prakash, and A. Khare, "Local energy-based multimodal medical image fusion in curvelet domain," *IET Comput. Vis.*, vol. 10, no. 6, pp. 513–527, Sep. 2016.

[3] L. Gondara. (2016). "Medical image denoising using convolutional denoising autoencoders." [Online]. Available: https://arxiv.org/abs/1608.04667

[4] J. M. Sanches, J. C. Nascimento, and J. S. Marques, "Medical image noise reduction using the SylvesterâŁ"Lyapunov equation," *IEEE Trans. Image Process.*, vol. 17, no. 9, pp. 1522–1539, Sep. 2008.

[5] J. Yuan, H. Chen, F. Sun, and Y. Huang, "Multisensor information fusion for people tracking with a mobile robot: A particle filtering approach," *IEEE Trans. Instrum. Meas.*, vol. 64, no. 9, pp. 2427–2442, Sep. 2015.

[6] Y. Zhang, Z. Xie, Z. Hu, S. Zhao, and H. Bai, "Online surface temperature measurement of billets in secondary cooling zone end-piece based on data fusion," *IEEE Trans. Instrum. Meas.*, vol. 63, no. 3, pp. 612–619, Mar. 2014.

[7] M. Manchandaa and R. Sharma, "A novel method of multimodal medical image fusion using fuzzy transform," *J. Vis. Commun. Image Represent.*, vol. 40, pp. 197–217, Oct. 2016.

[8] J. Du, W. Li, B. Xiao, and Q. Nawaz, "Union Laplacian pyramid with multiple features for medical image fusion," *Neurocomputing*, vol. 194, pp. 326–339, Jun. 2016.

[9] X. Xu, Y. Wang, and S. Chen, "Medical image fusion using discrete fractional wavelet transform," *Biomed. Signal Process. Control*, vol. 27, pp. 103–111, May 2016.

[10] Z. Liu, H. Yin, Y. Chai, and S. X. Yang, "A novel approach for multimodal medical image fusion," *Expert Syst. Appl.*, vol. 41, no. 16, pp. 7425–7435, 2014.

[11] R. Singh and A. Khare, "Fusion of multimodal medical images using Daubechies complex wavelet transform—A multiresolution approach," *Inf. Fusion*, vol. 19, pp. 49–60, Sep. 2014.

[12] X. Liu, W. Mei, and H. Du, "Multimodality medical image fusion algorithm based on gradient minimization smoothing filter and pulse coupled neural network," *Biomed. Signal Process. Control*, vol. 30, pp. 140–148, Sep. 2016.

[13] G. Bhatnagar, Q. M. J. Wu, and Z. Liu, "A new contrast based multimodal medical image fusion framework," *Neurocomputing*, vol. 157, pp. 143–152, Jun. 2015.

[14] Z. Xu, "Medical image fusion using multi-level local extrema," *Inf. Fusion*, vol. 19, no. 11, pp. 38–48, 2013.

[15] S. Li and L. Fang, "Signal denoising with random refined orthogonal matching pursuit," *IEEE Trans. Instrum. Meas.*, vol. 61, no. 1, pp. 26–34, Jan. 2012.

[16] I. Firoiu, C. Nafornita, J. M. Boucher, and A. Isar, "Image denoising using a new implementation of the hyperanalytic wavelet transform," *IEEE Trans. Instrum. Meas.*, vol. 58, no. 8, pp. 2410–2416, Aug. 2009.

[17] F. Russo, "Technique for image denoising based on adaptive piecewise linear filters and automatic parameter tuning," *IEEE Trans. Instrum. Meas.*, vol. 55, no. 4, pp. 1362–1367, Aug. 2006.

[18] Q. Guo, C. Zhang, Y. Zhang, and H. Liu, "An efficient SVD-based method for image denoising," *IEEE Trans. Circuits Syst. Video Technol.*, vol. 26, no. 5, pp. 868–880, May 2016.

[19] R. Sharma and M. Pavel, "Adaptive and statistical image fusion," in *Soc. Inf. Display Dig.*, vol. 17. 1996, pp. 969–972.

[20] A. M. Achim, C. N. Canagarajah, and D. R. Bull, "Complex wavelet domain image fusion based on fractional lower order moments," in *Proc. 8th Int. Conf. Inf. Fusion*, Jul. 2005, pp. 515–521.

[21] B. Yang and S. Li, "Multifocus image fusion and restoration with sparse representation," *IEEE Trans. Instrum. Meas.*, vol. 59, no. 4, pp. 884–892, Apr. 2010.

[22] S. Li, H. Yin, and L. Fang, "Group-sparse representation with dictionary learning for medical image denoising and fusion," *IEEE Trans. Biomed. Eng.*, vol. 59, no. 12, pp. 3450–3459, Dec. 2012.

[23] P. Scheunders and S. D. Backer, "Wavelet denoising of multicomponent images using Gaussian scale mixture models and a noise-free image as priors," *IEEE Trans. Image Process.*, vol. 16, no. 7, pp. 1865–1872, Jul. 2007.

[24] A. Loza, D. Bull, N. Canagarajah, and A. Achim, "Non-Gaussian model-based fusion of noisy images in the wavelet domain," *Comput. Vis. Image Understand.*, vol. 114, no. 1, pp. 54–65, 2010.

[25] W.-W. Wang, P.-L. Shui, and X.-C. Feng, "Variational models for fusion and denoising of multifocus images," *IEEE Signal Process. Lett.*, vol. 15, pp. 65–68, Jan. 2008.

[26] M. Kumar and S. Dass, "A total variation-based algorithm for pixel-level image fusion," *IEEE Trans. Image Process.*, vol. 18, no. 9, pp. 2137–2143, Sep. 2009.

[27] T. F. Chan, S. Esedoglu, and F. Park, "A fourth order dual method for staircase reduction in texture extraction and image restoration problems," in *Proc. IEEE Int. Conf. Image Process.*, Sep. 2010, pp. 4137–4140.

[28] R. K. Sharma, T. K. Leen, and M. Pavel, "Probabilistic image sensor fusion," in *Advances in Neural Information Processing Systems*, vol. 11. Cambridge, MA, USA: MIT Press, 1999, pp. 4137–4140.

[29] X. Bai, F. Zhou, and B. Xue, "Noise-suppressed image enhancement using multiscale top-hat selection transform through region extraction," *Appl. Opt.*, vol. 51, no. 3, pp. 338–347, 2012.

[30] X. Bai, F. Zhou, and B. Xue, "Fusion of infrared and visual images through region extraction by using multi scale center-surround top-hat transform," *Opt. Exp.*, vol. 19, no. 9, pp. 8444–8457, 2011.

[31] B. Chanda, M. K. Kundu, and Y. V. Padmaja, "A multi-scale morphologic edge detector," *Pattern Recognit.*, vol. 31, no. 10, pp. 1469–1478, 1998.

[32] D. Caixia *et al.*, "The improved algorithm of edge detection based on mathematics morphology," in *Proc. Int. J. Signal Process., Image Process. Pattern Recognit.*, vol. 7, no. 5, pp. 309–322, 2014.

[33] N. Bouaynaya and D. Schonfeld, "Theoretical foundations of spatially-variant mathematical morphology part II: Gray-level images," *IEEE Trans. Pattern Anal. Mach. Intell.*, vol. 30, no. 5, pp. 837–850, May 2008.

[34] S. R. Sternberg, "Grayscale morphology," *Comput. Vis., Graph., Image Understand.*, vol. 35, no. 3, pp. 333–355, 1986.

[35] Z. Dechun, P. Chenglin, C. Yuanyuan, "An improved morphological edge detection algorithm of medical image," *J. Chong Qing Univ.*, vol. 33, no. 2, pp. 123-126, 2010.

[36] S. Li, X. Kang, and J. Hu, "Image fusion with guided filtering," *IEEE Trans. Image Process.*, vol. 22, no. 7, pp. 2864–2875, Jul. 2013.

[37] E. S. L. Gastal and M. M. Oliveira, "Domain transform for edge-aware image and video processing," *ACM Trans. Graph.*, vol. 30, no. 4, p. 69, 2011.

[38] T. F. Chan and J. Shen, "Mathematical models for local nontexture inpaintings," *SIAM J. Appl. Math.*, vol. 62, no. 3, pp. 1019–1043, 2002.

[39] M. Bertalmio, G. Sapiro, V. Caselles, and C. Ballester, "Image inpainting," in *Proc. ACM SIGGRAPH*, 2000, pp. 417–424.

[40] P. Balasubramaniam and V. P. Ananthi, "Image fusion using intuitionistic fuzzy sets," *Inf. Fusion*, vol. 20, no. 15, pp. 21–30, 2014.

[41] G. Cui, H. Feng, Z. Xu, Q. Li, and Y. Chen, "Detail preserved fusion of visible and infrared images using regional saliency extraction and multi-scale image decomposition," *Opt. Commun.*, vol. 341, pp. 199–209, Apr. 2015.

[42] C. S. Xydeas and V. Petrović, "Objective image fusion performance measure," *Electron. Lett.*, vol. 36, no. 4, pp. 308–309, 2000.

[43] *Image Fusion Dataset*, accessed on Oct. 2016. [Online]. Available: http://www.imagefusion.org/

[44] *The Whole Brain*, accessed on Oct. 2016. [Online]. Available: http://www.med.harvard.edu/aanlib/home.html/

[45] V. Katkovnik, A. Foi, K. Egiazarian, and J. Astola, "From local kernel to nonlocal multiple-model image denoising," *Int. J. Comput. Vis.*, vol. 86, no. 1, pp. 1–32, 2010.

[46] *Image Fusion Toolbox for MATLAB 5.X*, accessed on Oct. 2016. [Online]. Available: http://www.metapix.de/toolbox.htm/

[47] T. M. Tu, S. C. Su, H. C. Shyu, and P. S. Huang, "A new look at IHS-like image fusion methods," *Inf. Fusion*, vol. 2, no. 3, pp. 177–186, 2001.

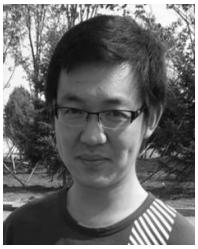

Wenda Zhao received the B.S. degree from Jilin University, Changchun, China, in 2011, and the Ph.D. degree from the Changchun Institute of Optics, Fine Mechanics and Physics, Chinese Academy of Sciences, Changchun, in 2016.

He is currently a Faculty with the School of Information and Communication Engineering, Dalian University of Technology, Dalian, China. His current research interests include image fusion and object tracking.

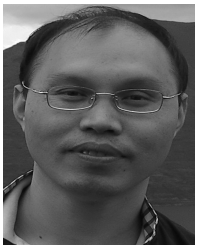

Huchuan Lu (SM'12) received the M.S. degree in signal and information processing and the Ph.D. degree in system engineering from the Dalian University of Technology (DUT), Dalian, China, in 1998 and 2008, respectively.

He has been a Faculty since 1998 and a Professor since 2012 with the School of Information and Communication Engineering, DUT. His current research interests include computer vision and pattern recognition and visual tracking and segmentation.

Dr. Lu is an Associate Editor of the IEEE TRANSACTIONS ON SYSTEMS, MAN, AND CYBERNETICS: PART B.